Stress Concentration in the Aortic Wall due to Patient-Specific Calcification Inclusion

Stewart McLennan (1) ✉, **Gilles Soulez** (2), **Simon Lessard** (2), **Helena Strube** (1), **Rosaire Mongrain** (1)

1. McGill University, Canada; 2. Université de Montréal, Canada

Date: April 30, 2020

Location: Virtual Seminar 2020

✉ stewart.mclennan@mail.mcgill.ca

Département de radiologie, radio-oncologie et médecine nucléaire
Faculté de médecine
Université de Montréal

Disclosures

The research project was supported by the Nature Sciences and Engineering Research Council of Canada (NSERC) collaborative research and development grant, in partnership with Siemens Healthineers.

Département de radiologie, radio-oncologie
et médecine nucléaire
Faculté de médecine
Université de Montréal

Introduction

Aorta Wall Calcification

Atherosclerotic calcification in major vessel beds is associated with an increased risk of death [1]. Experimental study into the mechanical properties of Abdominal Aortic Aneurysm (AAA) calcification is limited despite research showing that most AAAs contain a noticeable amount of calcification [2]. There is debate over the relationship between calcification and aneurysm rupture risk, with some suggesting calcification leads to wall stress concentration which promotes rupture and others suggesting the stiffness of calcification helps stabilize the wall, preventing rupture.

Endovascular Aneurysm Repair Simulation

In 2017 in the United States, AAA related complications were responsible for 9,928 deaths, with a crude death rate of 3 per 100,000 [3]. Endovascular intervention became a common alternative to open surgery by the 1990s, demonstrating improved clinical outcomes over open techniques including faster recovery times and improved mortality rates [4]. The current practice of Endovascular Aneurysm Repair (EVAR) is limited by a number of factors including exposure to high doses of X-ray radiation, limited 3D imaging, and lack of contact force sensing from the endovascular tools and the vascular anatomy [4]. To properly deliver the prostheses, fluoroscopic image guidance can be enhanced using image registration approaches, however during the insertion of the endovascular tools, the vascular system undergoes significant deformations which degrades image registration accuracy [5]. As a consequence, there remains a need to verify the accuracy of the overlaid features by additional intraoperative imaging and consequently added doses of the contrast medium to perform the necessary adjustments [6, 7]. It has been shown that Finite Element Analysis (FEA) is feasible and reproducible in simulating device-to-tissue interactions and quantifying anatomic deformations during EVAR [6].

Methods

To assess the role of calcification in both vascular stress concentration and EVAR simulation accuracy, a FEA model components were developed as outlined below.

Calcification

The calcification was modelled as a Mooney-Rivlin rubber material, with parameters D1=18.804.5 Pa and D2=20 [8].

Aorta

The vascular wall was modelled as a second order Yeoh hyperelastic, homogenous, isotropic, and incompressible material model based on Raghavan et al. [9].

Intraluminal Thrombus

The intraluminal thrombus (ILT) was modeled as a single layered incompressible tissue using the one parameter Ogden-like strain energy function [10].

Bone

The bone component of the model was characterized using a linear elastic material with a Young's modulus of 17GPa and a Poisson ratio of 0.3 [11].

Abdomen

Data from Sommer et al. [12] was fitted using the Levenberg-Marquardt nonlinear regression method, to establish material parameters of the second order Yeoh hyperelastic material strain energy function for long-time elastic response of perivascular adipose tissue (PVAT).

Delivery Tools

The guidewire and delivery device components were modelled as linear elastic (Poisson's ratio of 0.3, guidewire Young's modulus of $2.03 \times 10^8 \pm 1.09 \times 10^6$kPa, and delivery device Young's modulus of $3.40 \times 10^5 \pm 4.70 \times 10^4$kPa to $9.21 \times 10^5 \pm 6.60 \times 10^4$kPa) [6].

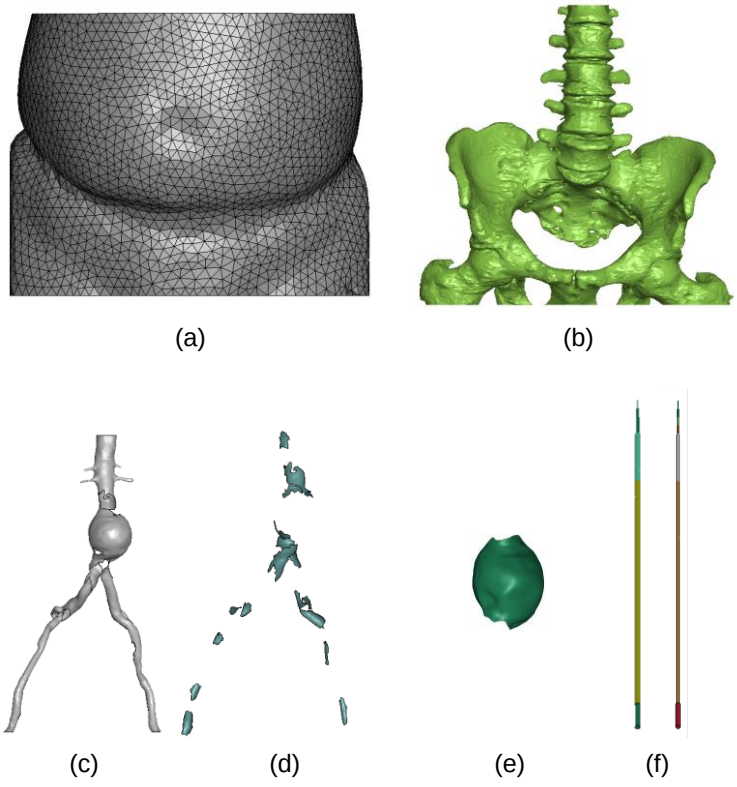

Figure 1 Meshed model parts: (a) Abdomen (b) Bone (c) Aorta wall (d) Calcification (e) Intraluminal thrombus (f) Stent-graft delivery tools.

Département de radiologie, radio-oncologie et médecine nucléaire
Faculté de médecine
Université de Montréal

Methods

Segmentation

The aorto-iliac arteries, spinal column, PVAT and pelvic bones were segmented using CT-scan geometries using a semi-automated 3D segmentation tool (ITK-SNAP) while the volume of ILT was segmented using the ORS segmentation software (Object Research System Montreal, Quebec, Canada). The aorta was reconstructed from the celiac-aorta to the distal level of inguinal ligament in the femoral triangle.

Boundary Conditions

For model boundary conditions, imposed fixed supports were applied at the bottom ends of the iliac arteries and the top of the aorta. The top support represented the physiological restraint caused by the aortic hiatus on the proximal extremity of the aortoiliac structure in coeliac aorta. Similarly, the bottom support represented the lateral collateral and inguinal ligaments which hold the distal extremity in the femoral triangle stationary. The boundary edges of the perivascular tissues medium were also fixed.

Frictionless contact was defined between the tools and the arterial wall while the aorta, ILT, PVAT and bone were assigned tied contact properties.

To represent the pre-stressed state of the aorta, the inverse approach strategy as presented by Bols et al. [13] was used.

Mesh

The aorta and calcification parts was discretized into three-node triangular shell elements with a mean characteristic size of 1.5mm while four-node tetrahedral elements, also with mean characteristic length of 1.5mm, were used to discretize the bone, ILT and PVAT parts. The delivery tools were discretized into two-node beam elements.

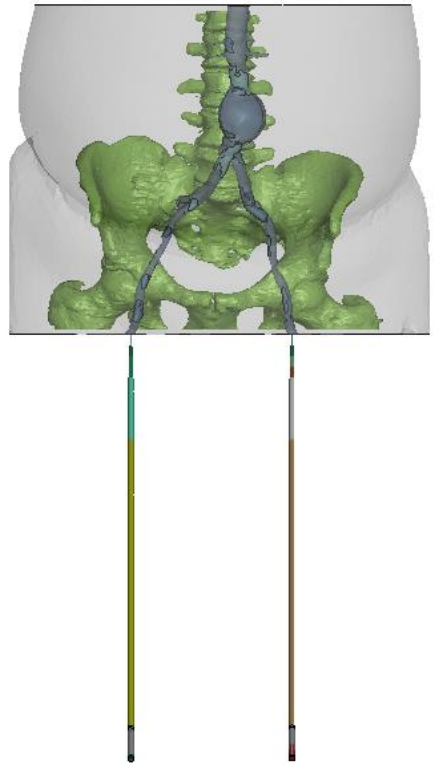

Figure 2 Fully constructed FEA model.

Département de radiologie, radio-oncologie
et médecine nucléaire
Faculté de médecine
Université de Montréal

Methods

Stress Concentration

Aorta calcification was segmented from CT-scans of ten patients having already undergone EVAR (CHUM Hospital, Montreal, QC, Canada), who exhibited moderate to severe calcification presence. The calcification geometry was then meshed (Meshmixer 3.5). For each patient a ‘Non-calcified’ and ‘Calcified’ model was created to assess the impact of calcification inclusion on peak wall stress, average wall stress and stress concentration.

Endovascular Aneurysm Repair Simulation

Additionally, to assess the impact of calcification inclusion in preoperative and intraoperative clinical simulation tools, we overlaid the three-dimensional FEA output geometry of the guidewires and aorta wall on intraoperative CT-scan images of the respective patients. Misregistration between the simulated and real guidewire centrelines and ostia junctions were recorded for each patient in accordance with the method used by Kauffmann et al. [5].

For each patient, three different model variations were assessed: ‘Non-calcified - simple geometry abdomen’, ‘Non-calcified - patient-specific geometry abdomen’, and ‘Calcified - patient-specific geometry abdomen’. This enabled us to individually assess both the image registration improvement for inclusion of the patient-specific geometry abdomen and calcification in each model.

Figure 3 shows the overlaid images for patient number 10, with the dotted lines and blue markers representing the simulated geometry locations for the guidewire centrelines and ostia junctions, respectively. These landmarks enabled measurement of error between the intraoperative image and simulation overlay at predetermined landmarks.

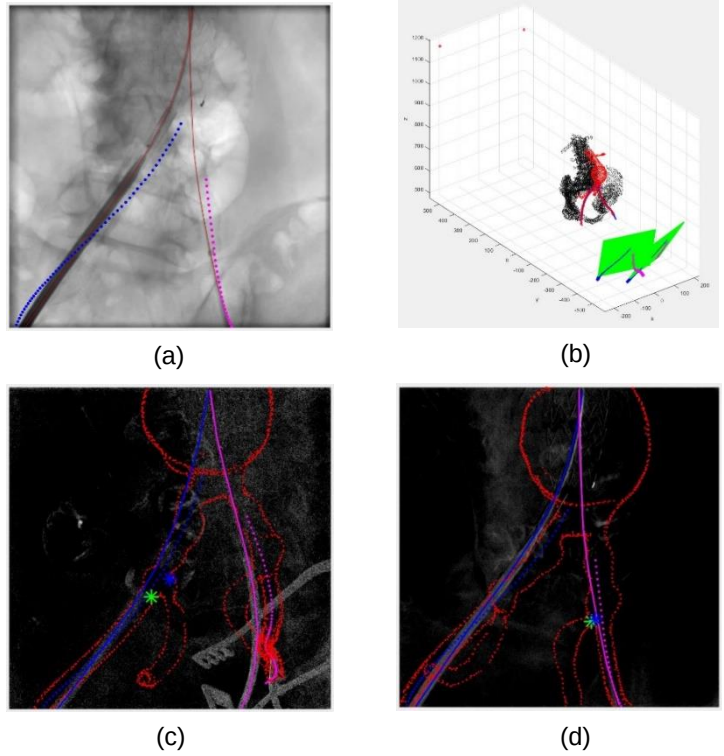

Figure 3 Patient 10 registration overlays: (a) Guidewire centrelines (b) Image projection (c) Right ostia (d) Left Ostia.

Département de radiologie, radio-oncologie
et médecine nucléaire
Faculté de médecine
Université de Montréal

Results – Stress Concentration

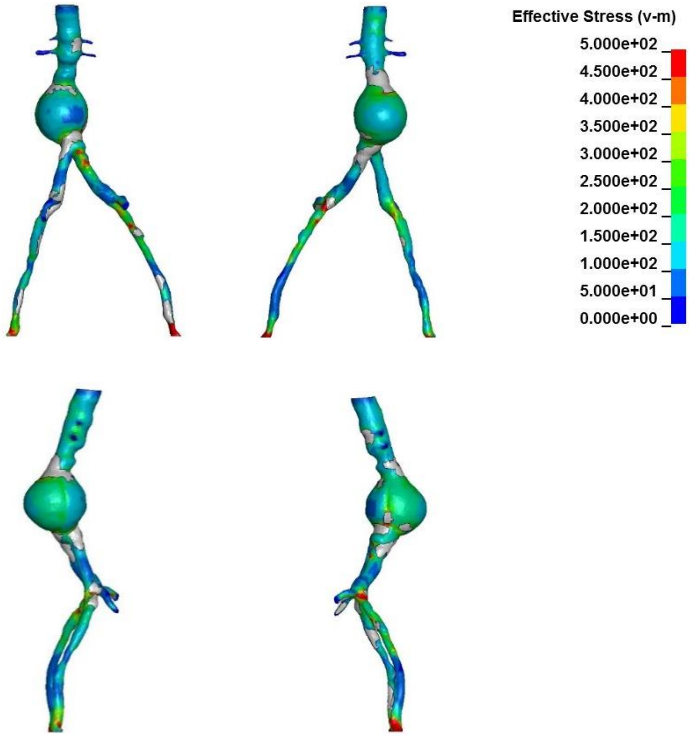

Figure 4 Von Mises Stress (VMS) response (kPa) of aorta wall under peak blood pressure loading.

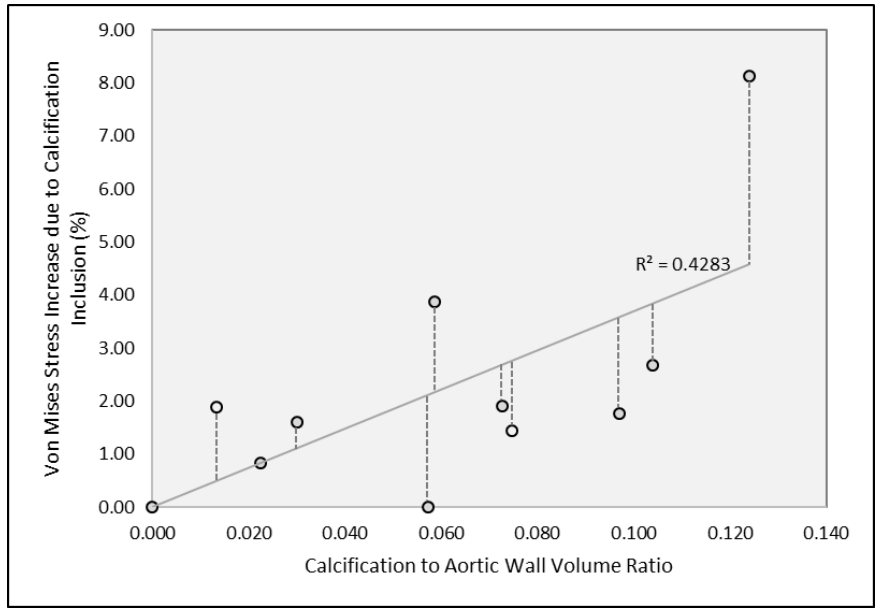

Figure 5 Correlation plot between Von Mises Stress increase and volumetric ratio of calcification to aortic wall.

Département de radiologie, radio-oncologie et médecine nucléaire
Faculté de médecine
Université de Montréal

Results – Endovascular Aneurysm Repair Simulation

Patient	Patient-Specific Abdomen Inclusion Improvement (%)	Calcification Inclusion Improvement (%)	Calcification /Aorta Wall Ratio
1	4.28	7.06	0.013
2	-0.89	1.83	0.023
3	2.00	2.57	0.030
4	16.73	7.09	0.057
5	3.36	4.31	0.059
6	-1.78	10.05	0.073
7	26.48	15.25	0.075
8	-6.93	8.63	0.097
9	-3.68	11.14	0.104
10	-5.42	10.78	0.124
Average	3.41	7.87	

Table 1 Registration improvement data in relation to volumetric ratio of calcification to aortic wall, for both patient-specific abdomen and calcification inclusion.

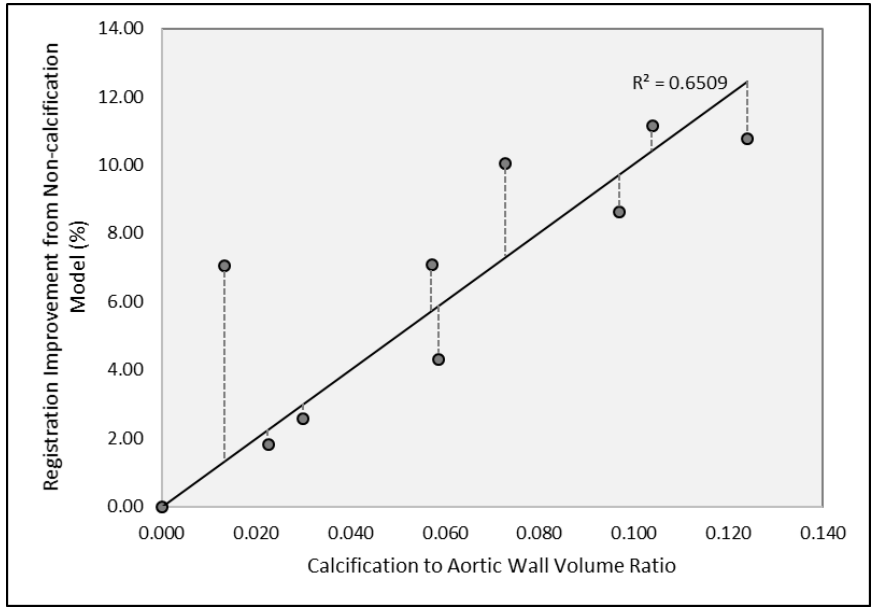

Figure 6 Correlation plot between registration improvement volumetric ratio of calcification to aortic wall.

Département de radiologie, radio-oncologie et médecine nucléaire
Faculté de médecine
Université de Montréal

Discussion

Stress Concentration

Calcification inclusion within the FEA models produced higher average VMS in the aorta wall (109.26 vs 106.66kPa, n=10), suggesting calcification may be a factor in terms of increased aneurysm rupture risk due to greater stress on the aorta wall. In addition, the greater the volumetric ratio of calcification for the patient lead to a greater increase in average VMS ($p<0.05$).

Figure 4 highlights how the peak wall stresses localize around the calcification regions. This is to be expected, as in reality, calcified aorta wall is known to be less compliant than healthy aorta wall. As such, healthy aorta wall around calcified regions experience greater deformation to ensure artery compliance which leads to greater stress concentration.

Although not presented here, we performed a validation study using a simplified aorta FEA model to assess the impact of calcification geometry. We investigated the impact on wall mechanical behaviour when using patient-specific calcification geometry over idealized calcification geometry. It was found that using patient-specific calcification geometry lead to a significant increase in peak wall VMS (585.61kPa vs 28.63kPa, n=4). As such, real calcification geometries were included in the FEA models of the present study.

Endovascular Aneurysm Repair Simulation

A significant correlation was found between patient-specific calcification inclusion in EVAR simulations and there registration accuracy for intraoperative use ($p<0.005$). This suggests that for simulation studies using patients with heavy calcification presence, calcification is an important inclusion.

A limitation of this study is that certain body components such as the rib cage and organs surrounding the aorta were excluded from the FEA models due to computational cost. Ideally these should be included in order to produce a more complete simulation. Additionally, the time taken to develop and run the models for each individual patient is impractical for clinical usage, as such future research should seek to optimize the development and running process while maintaining simulation accuracy.

Conclusion

The results of this study suggest that calcification plays a significant role in the mechanical behavior of the aorta wall. Although not definitive, the results suggest fractures may propagate at areas of aorta tissue in close proximity to calcified tissue.

The results confirmed the feasibility of the model for predicting the vascular wall and endovascular tool deformations during an EVAR procedure. After verifying the reliability of the model on a larger number of patients and performing optimization, it can potentially be used for matching of preoperative data and intraoperative images to provide practitioners with an accurate road mapping tool while minimizing the patient exposure to harmful contrast agents.

Future research may focus on the impact of calcification presence on stent-graft attachment, deformation and fracture following EVAR intervention. This would provide important data regarding post-operative EVAR complications.

Although the focus of this study is on abdominal aneurysm treatment, the biomechanical framework of the presented work is applicable to a number of other interventional endovascular procedures such as treatment of cerebral aneurysms.

References

1. Bos D, Leening MJG, Kavousi M, Hofman A, Franco OH, van der Lugt A, Vernooij MW, Ikram MA: **Comparison of Atherosclerotic Calcification in Major Vessel Beds on the Risk of All-Cause and Cause-Specific Mortality**. *Circulation: Cardiovascular Imaging* 2015, **8**(12):1-9.
2. Kaladji A, Dumenil A, Castro M, Cardon A, Becquemin J-P, Bou-Saïd B, Lucas A, Haigron P: **Prediction of deformations during endovascular aortic aneurysm repair using finite element simulation**. *Computerized Medical Imaging and Graphics* 2013, **37**(2):142-149.
3. Centers for Disease Control and Prevention, and National Center for Health Statistics: **Underlying Cause of Death. 1999-2017** on CDC WONDER Online Database, released December, 2018. *Available at: http://wonder.cdc.gov/ucd-icd10.html View in Article* (2019).
4. Rafii-Tari H, Payne C, Yang G-Z: **Current and Emerging Robot-Assisted Endovascular Catheterization Technologies: A Review**. *Annals of Biomedical Engineering* 2013, **42**.
5. Kauffmann C, Douane F, Therasse E, Lessard S, Elkouri S, Gilbert P, Beaudoin N, Pfister M, Blair JF, Soulez G: **Source of Errors and Accuracy of a Two-Dimensional/Three-Dimensional Fusion Road Map for Endovascular Aneurysm Repair of Abdominal Aortic Aneurysm**. *Journal of Vascular and Interventional Radiology* 2015, **26**(4):544-551.
6. Mohammadi H, Lessard S, Therasse E, Mongrain R, Soulez G: **A Numerical Preoperative Planning Model to Predict Arterial Deformations in Endovascular Aortic Aneurysm Repair**. *Annals of Biomedical Engineering* 2018, **46**(12):2148-2161.
7. Lessard S, Kauffmann C, Pfister M, Cloutier G, Thérasse É, de Guise JA, Soulez G: **Automatic detection of selective arterial devices for advanced visualization during abdominal aortic aneurysm endovascular repair**. *Medical Engineering & Physics* 2015, **37**(10):979-986.
8. Li Z-Y, U-King-Im J, Tang TY, Soh E, See TK, Gillard JH: **Impact of calcification and intraluminal thrombus on the computed wall stresses of abdominal aortic aneurysm**. *Journal of Vascular Surgery* 2008, **47**(5):928-935.
9. Raghavan ML, Vorp DA: **Toward a biomechanical tool to evaluate rupture potential of abdominal aortic aneurysm: identification of a finite strain constitutive model and evaluation of its applicability**. *Journal of Biomechanics* 2000, **33**(4):475-482.
10. Gasser TC, Görgülü G, Folkesson M, Swedenborg J: **Failure properties of intraluminal thrombus in abdominal aortic aneurysm under static and pulsating mechanical loads**. *Journal of Vascular Surgery* 2008, **48**(1):179-188.
11. Dalstra M, Huiskes R, van Erning L: **Development and validation of a three-dimensional finite element model of the pelvic bone**. *J Biomech Eng* 1995, **117**(3):272-278.
12. Sommer G, Eder M, Kovacs L, Pathak H, Bonitz L, Mueller C, Regitnig P, Holzapfel GA: **Multiaxial mechanical properties and constitutive modeling of human adipose tissue: A basis for preoperative simulations in plastic and reconstructive surgery**. *Acta Biomaterialia* 2013, **9**(11):9036-9048.
13. Bols J, Degroote J, Trachet B, Verhegghe B, Segers P, Vierendeels J: **A computational method to assess the in vivo stresses and unloaded configuration of patient-specific blood vessels**. *Journal of Computational and Applied Mathematics* 2013, **246**:10-17.